


Large Spin-Orbit-Torque Efficiency Generated by Spin Hall Effect in Paramagnetic Co-Ni-B Alloys

Y. Hibino¹,* T. Taniguchi¹, K. Yakushiji, A. Fukushima¹, H. Kubota¹, and S. Yuasa
Research Center for Emerging Computing Technologies, National Institute of Advanced Industrial Science and Technologies (AIST), Tsukuba, Ibaraki 305-8568, Japan

 (Received 4 September 2020; revised 2 November 2020; accepted 20 November 2020; published 17 December 2020)

The spin Hall effect is a major source of spin-orbit torques (SOTs), which allow efficient electrical manipulation of magnetization. So far, the spin Hall effect has been investigated using materials with strong spin-orbit coupling, such as $5d$ transition metals, and the spin Hall effect in light elements, which results in weak spin-orbit coupling, is often considered to be negligible. Here, we report an efficient spin Hall material that can be realized using $3d$ transition metals, namely, an amorphous Co-Ni-B alloy under a paramagnetic state. Despite no heavy elements being used in this material, we estimate the spin Hall angle of Co-Ni-B alloys to be about 0.10 via harmonic Hall measurements, which is comparable to that of $5d$ transition metals. A highly efficient spin Hall angle originates from the high-spin Hall conductivity of paramagnetic Ni. We also demonstrate SOT-induced magnetization switching using the spin Hall effect on the Co-Ni-B alloy with comparable switching current density using a heavy-metal spin Hall material. Our findings provide an approach to realize the coexistence between highly efficient and heavy-element-free SOT-based devices.

DOI: [10.1103/PhysRevApplied.14.064056](https://doi.org/10.1103/PhysRevApplied.14.064056)

I. INTRODUCTION

Spin-orbit torques (SOTs) induced by in-plane electrical injection have been intensively studied because of their potentially efficient way of controlling magnetization dynamics [1–4]. The basic structure of a SOT-based device consists of normal-metal (NM) and ferromagnet (FM) bilayers and phenomena induced by spin-orbit coupling [e.g., the spin Hall effect (SHE) in NM [3–5] and the Rashba-Edelstein effect (REE) at the NM/FM interface [2]] are considered to be the driving forces of SOT. There are two components of torques, dampinglike SOT (DL SOT) and fieldlike SOT (FL SOT). Currently, great effort has been made to enhance DL SOT efficiency per unit current density (ξ_{DL}) to achieve energy-efficient operations.

Using materials with a large SHE is one of the simplest ways to enhance ξ_{DL} . The key parameter that defines the strength of the SHE is the spin Hall angle, θ_{SHE} , which is defined as the ratio between generated spin current, j_s , and induced electrical charge current, j_e ($\theta_{SHE} = j_s/j_e$). Previous studies showed that spin Hall materials, such as Pt [6,7], W [8,9], and Pt-based binary alloys [10,11], achieved a relatively high spin Hall angle. These studies focused on heavy metals ($5d$ or $4d$ transition metals) because the strength of the spin-orbit coupling could be scaled with atomic number, Z . Spin Hall materials that use

heavy metals have a high application cost; therefore, creating materials that obtain weak spin-orbit coupling and a large SHE concurrently is imperative. Naito *et al.* and Jo *et al.* used tight-binding model calculations to predict a sizable SHE in $3d$ transition metals, which are considered to have weak spin-orbit coupling [12,13]. Furthermore, recent experiments revealed that $3d$ transition metals, such as Cr [14] and V [15], show a sizable spin Hall effect (or inverse spin Hall effect) with spin Hall angles as large as -0.05 and -0.07 , respectively.

Here, we focus on the SHE in nickel (Ni) because previous tight-binding model calculation results show that the spin Hall conductivity of Ni can be as large as $10^3 \Omega^{-1}\text{cm}^{-1}$, which is comparable to that of Pt [12,13]. Furthermore, spin Hall conductivity is unaffected by the magnetic state (i.e., ferromagnetic state and paramagnetic state) of Ni, indicating the importance of the intrinsic mechanism from the electronic band structure [13]. Moreover, Keller *et al.* recently used a spin-pumping measurement to find a relatively large spin Hall effect in paramagnetic Ni-Cu binary alloys [16]. Here, we focus on amorphous Co-Ni-B alloys as potential paramagnetic Ni-based materials, the amorphous structure of which greatly reduces the phase transition temperature of the paramagnetic state to the ferromagnetic state [17,18]. We reveal that the spin Hall angle (spin Hall conductivity) of the paramagnetic Co-Ni-B alloy can reach up to about 0.1 ($\sim 10^3 \Omega^{-1}\text{cm}^{-1}$) with a spin diffusion length of about 2.0 nm. We reveal that the large spin Hall

*y-hibino@aist.go.jp

angle is attributed to the combination of a large spin Hall conductivity in paramagnetic Ni, consistent with the previous calculation results. We also demonstrate SOT-induced magnetization switching using the spin Hall effect in the Co-Ni-B alloy and obtain a switching current density of about $1.5 \times 10^{11} \text{ A/m}^2$. These results show that the paramagnetic Ni-based alloy is a good candidate of SOT-based devices without heavy metals being used.

II. RESULTS AND DISCUSSION

A. Co-Ni-B alloy

To obtain paramagnetic Co-Ni-B alloys, first, we prepare Co-Ni-B alloy films that contain various Co compositions. We use magnetic stacks on thermally oxidized Si substrates by utilizing ultrahigh vacuum magnetron sputtering, as follows: substrate/Ta(2)/(Co_xNi_{1-x})₈₀B₂₀(10)/Ta(5). The numbers in parentheses indicate the thickness of each layer in nanometers. We make Co-Ni-B alloys by cosputtering the Co₈₀B₂₀ and Ni₈₀B₂₀ targets at various sputtering powers, and we calculate the Co composition, x , by the deposition rate of each target. We use x-ray diffraction (XRD) measurements to confirm that all Co-Ni-B alloy samples have an amorphous structure. Notably, all magnetic stacks referred to hereafter are prepared by same method.

In Fig. 1(a), we show the magnetization curve of various x samples measured at room temperature. The $x = 15.1\%$ sample shows a linear response to the magnetic field, indicating paramagnetic behavior. By increasing x , we observe a clear hysteresis curve with a finite saturation magnetic moment that shows ferromagnetic behavior in the Co-rich region. From the x dependence on the saturation magnetization [see Fig. 1(b)], we find that the Co-Ni-B alloys are in the paramagnetic state in the $x < 25\%$ region. The paramagnetic behavior in the Ni-rich region is consistent with previous work on amorphous Co-Ni-based alloys [17,18]. In the next section, we discuss using Co-Ni-B alloys with $x < 25$.

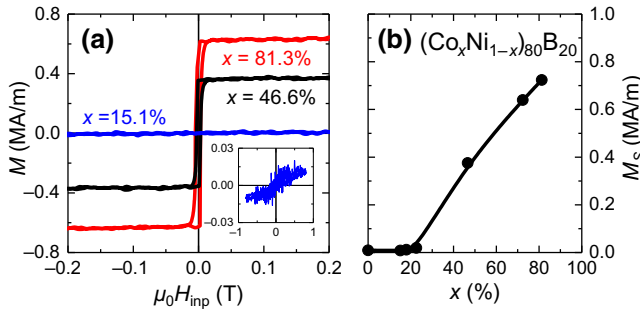


FIG. 1. Magnetic properties of Co-Ni-B alloy. (a) Magnetization curve of various Co compositions, x , under in-plane magnetic field, H_{inp} . Inset shows a magnified view of $x = 15.1\%$ sample. (b) x dependence of saturation magnetization, M_s .

B. Spin Hall effect in paramagnetic Co-Ni-B

To estimate the SOT generated from the spin Hall effect in paramagnetic Co-Ni-B alloys, we prepare the following magnetic stacks [see Fig. 2(a)]: substrate/Ta(2)/CNB(t_{CNB})/Cu-N(1)/Fe-B(1.4)/MgO/TaOx(2). Here, CNB refers to Co-Ni-B alloys with $x = 14.9\%$, and its thickness, t_{CNB} , varies between 2 and 12 nm. We insert 1-nm-thick Cu-N between the CNB and Fe-B layers to exclude the exchange interaction between the two layers. We pattern magnetic stacks into $10\text{-}\mu\text{m}$ -wide Hall bars using a standard optical lithography technique and ion-beam etching. To ensure the electrical contacts, we fabricate Cr(5)/Au(100) electrodes with a lift-off process. All measurements are conducted at room temperature.

First, we investigate the fundamental magnetic properties of the magnetic stacks shown above. In Fig. 2(a), we show the Hall resistance curve of three different t_{CNB} samples. All samples show a linear increase with the out-of-plane magnetic field, H_z , and saturate near 350 mT, indicating that the Fe-B layer in our system is in-plane magnetized. As Fig. 2(a) shows, we estimate the anomalous Hall resistance, R_{AHE} , as shown in Fig. 2(b). R_{AHE} decreases with t_{CNB} because the shunting current ratio in Fe-B decreases as t_{CNB} increases. We also measure the planar Hall resistance (R_{PHE}) by measuring the magnetoresistance under a rotating fixed external magnetic field, H_{ext} , along the x - y plane (φ -scan measurements). We estimate the effective demagnetization field, H_{demag} , and the damping constant, α , of the Fe-B layer from the ferromagnetic resonance measurement shown in Fig. 2(c). H_{demag} is estimated to be about 350 mT in all samples, which is consistent with the Hall resistance curve shown in Fig. 2(a). The value α of all samples is about 0.01, which is lower than that of Pt/Ni-Fe (Co) [6,7], but higher than that of Ta/Co-Fe-B [3,19]. Notably, the inhomogeneous broadening of the present system is about 0.2 mT in all samples, indicating low roughness of the Cu-N surface [20].

To estimate the SOT generated from the spin Hall effect on the CNB layer, we conduct harmonic Hall measurements [21,22] by using the circuit shown in Fig. 3(a). In this method, the SOT induced by the sinusoidal current oscillates the magnetization of Fe-B. This SOT-driven magnetization oscillation can be detected from the out-of-phase second-harmonic Hall resistance, R_H^{2f} . Figure 3(b) shows the φ -scan measurements of R_H^{2f} that are expressed as follows:

$$\begin{aligned}
 R_H^{2f} &= R_{\text{DL}} \cos \varphi + R_{\text{FL+Oe}} \cos 2\varphi \cos \varphi, \\
 R_{\text{DL}} &= -\frac{R_{\text{AHE}} H_{\text{DL}}}{2(H_{\text{ext}} + H_{\text{demag}})} + R_T, \\
 R_{\text{FL+Oe}} &= R_{\text{PHE}}(H_{\text{FL}} + H_{\text{Oe}})/H_{\text{ext}}.
 \end{aligned} \tag{1}$$

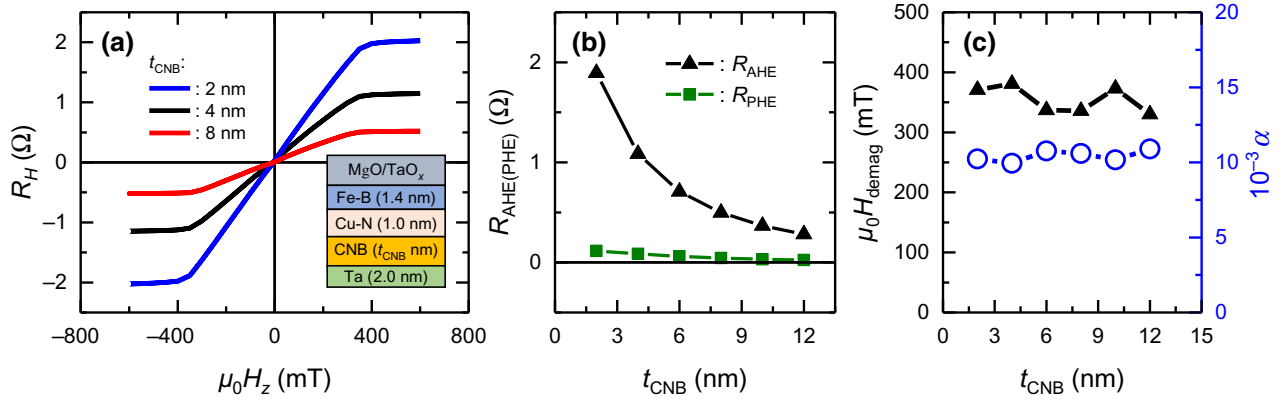


FIG. 2. Magnetic and electrical properties of CNB/Cu-N/Fe-B system. (a) Hall resistance curve of different CNB thickness, t_{CNB} , samples under out-of-plane magnetic field, H_z . μ_0 represents permeability under vacuum. Inset shows schematic of the magnetic stack. (b) t_{CNB} dependence of anomalous Hall resistance, R_{AHE} (black), and planar Hall resistance, R_{PHE} (green). (c) t_{CNB} dependence of effective demagnetization field, H_{demag} (solid black triangles), and damping constant, α (open blue circles).

Here, R_{DL} and R_{FL+Oe} are the fitting parameters. H_{DL} , H_{FL} , and H_{Oe} correspond to a current-induced effective field driven by the DL SOT, the FL SOT, and the Oersted field, respectively. R_T is an additional signal from a thermal-electric effect, such as the anomalous Nernst effect of Fe-B. To evaluate H_{DL} and $H_{FL}+H_{Oe}$ of the system, first, we fit the R_H^{2f} curve with Eq. (1) and obtain R_{DL} and R_{FL+Oe} , respectively. As Fig. 3(c) shows, we confirm that both components are proportional to the applied current, as expected from $H_{DL(FL+Oe)} \propto I_{ac}$.

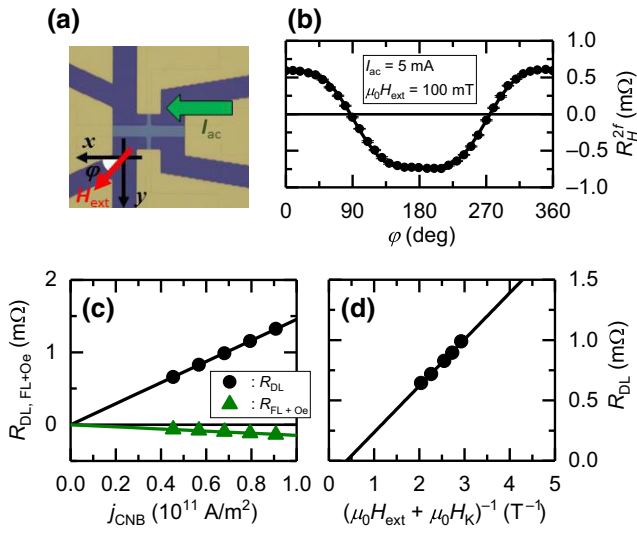


FIG. 3. Harmonic Hall measurement results with $t_{CNB} = 4$ nm. (a) Optical picture of fabricated Hall device and configuration of measurements. (b) φ -scan measurements of second-harmonic Hall resistance (R_H^{2f}) curve. Solid line corresponds to fitting using Eq. (1). (c) Current density dependence of R_{DL} and R_{FL+Oe} (solid line shows linear fitting). (d) R_{DL} as function of $(\mu_0 H_{ext} + \mu_0 H_K)^{-1}$. Solid line shows linear fitting.

Then, we estimate H_{DL} ($H_{FL}+H_{Oe}$) from the slope of the $\cos\varphi$ component ($\cos 2\varphi \cos\varphi$ component) as a function of $(H_{ext}+H_{demag})^{-1}$ (H_{ext}^{-1}), alternating H_{ext} and the applied current. We evaluate the DL SOT efficiency by $\xi_{DL} = -2eM_s t \mu_0 H_{DL} / \hbar j_{CNB}$, with e as the elementary charge, \hbar as the Dirac coefficient, j_{CNB} as the current density of the CNB layer, M_s as the saturation magnetization, and t as the thickness of the Fe-B layer.

Figure 4 shows the CNB thickness, t_{CNB} , dependence of ξ_{DL} . ξ_{DL} shows a monotonic increase and saturates up to about 8 nm. From this behavior, we consider that the spin current generated from interfacial effect at CNB/Cu-N [2,23] is negligible compared with the SHE in our system. Using the t_{CNB} dependence, we evaluate the effective spin Hall angle, θ_{SHE} , and spin-diffusion length, λ_s , which are important parameters for spin Hall materials. We evaluate θ_{SHE} and λ_s by fitting data with the following equation (solid curve = fitting results): $\xi_{DL} = \theta_{SHE}[1 - \text{sech}(t_{CNB}/\lambda_s)]$. The fitting yields $\theta_{SHE} = 10.5\%$

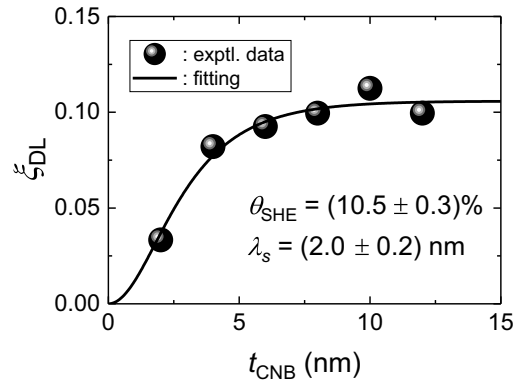


FIG. 4. CNB thickness dependence of DL SOT efficiency, ξ_{DL} . Solid line shows best ξ_{DL} fitting curve.

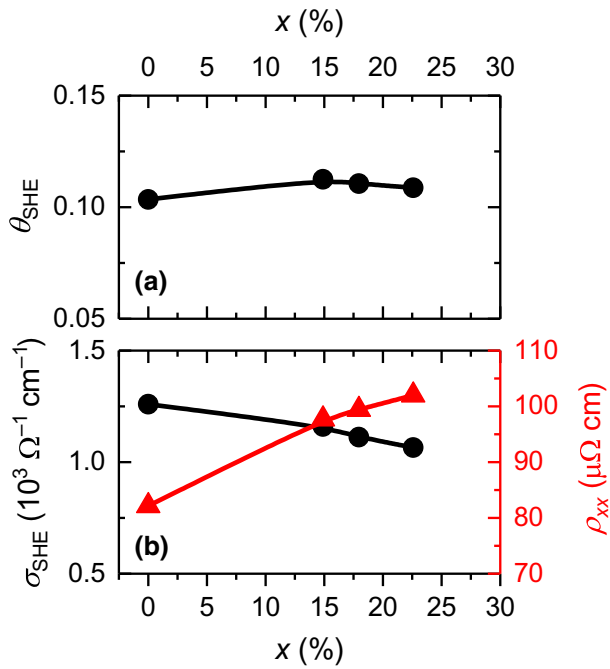


FIG. 5. Co composition, x , dependence of (a) effective spin Hall angle, θ_{SHE} ; (b) spin Hall conductivity, σ_{SHE} (left axis); and longitudinal resistivity, ρ_{xx} (right axis).

and $\lambda_s = 2.0$ nm. The estimated θ_{SHE} is comparable to that of $5d$ transition metals, such as Pt [6,21]. We assume that the spin Hall effect in Cu-N is negligible in the current system. To check the large spin Hall effect in CNB further, we calculate the spin Hall conductivity using $\sigma_{\text{SHE}} = \theta_{\text{SHE}}/\rho_{xx}$, where ρ_{xx} is the longitudinal resistivity of the CNB layer ($97.7 \mu\Omega \text{cm}$), and we estimate $\sigma_{\text{SHE}} = (+1.07 \pm 0.03) \times 10^3 \Omega^{-1} \text{cm}^{-1}$. This value is an order of magnitude larger than those of other $3d$ elements, such as Cr [14] and V [15]. In addition, the spin-torque efficiency obtained here is orders of magnitude larger than those of

the ferromagnetic $3d$ -alloy systems [23]. The estimated σ_{SHE} is similar in order of magnitude to that of the result calculated using the tight-binding model [12,13]. The spin-diffusion length of the CNB layer is shorter than that of other $3d$ elements [14,15], possibly because of the high longitudinal resistivity of the amorphous CNB.

Next, we investigate the effects of Co doping. Previous studies [13,24] showed that the spin Hall conductivity could be tuned by shifting the Fermi level through doping. Therefore, we study the Co composition dependence of the spin Hall angle, θ_{SHE} ; the spin Hall conductivity, σ_{SHE} ; and the longitudinal resistivity, ρ_{xx} , of Co-Ni-B alloy (as shown in Fig. 5). We prepare four magnetic stacks with four different values of x ($= 0, 14.9, 17.9,$ and 22.5%), and we set the Co-Ni-B layer thickness to 10 nm. The magnetic stack we use is the same as that in the inset of Fig. 2(a), except for the Co-Ni-B layer. θ_{SHE} shows a slight maximum at $x = 15\%$. Meanwhile, σ_{SHE} shows a monotonic decrease with x , indicating that the intrinsic mechanism in the Ni element plays an essential role in a large spin Hall effect and Co doping is inefficient. Previous calculations and experimental results show that the spin Hall conductivity in Co is smaller than that of Ni [12,25], which may explain our composition dependence. In addition, the monotonic decrease of σ_{SHE} indicates the negligible effect of spin-fluctuation enhancement of the SHE in our Co-Ni-B alloys at room temperature [26,27]. The slight enhancement of θ_{SHE} at $x = 15.1\%$ can be understood from the monotonic increase of ρ_{xx} , with x originating from impurity scattering because θ_{SHE} is a product of σ_{SHE} and ρ_{xx} .

C. SOT-induced magnetization switching

Lastly, we show the SOT-induced magnetization switching using CNB as a spin Hall material. We prepare a perpendicularly magnetized Fe-B layer system as follows

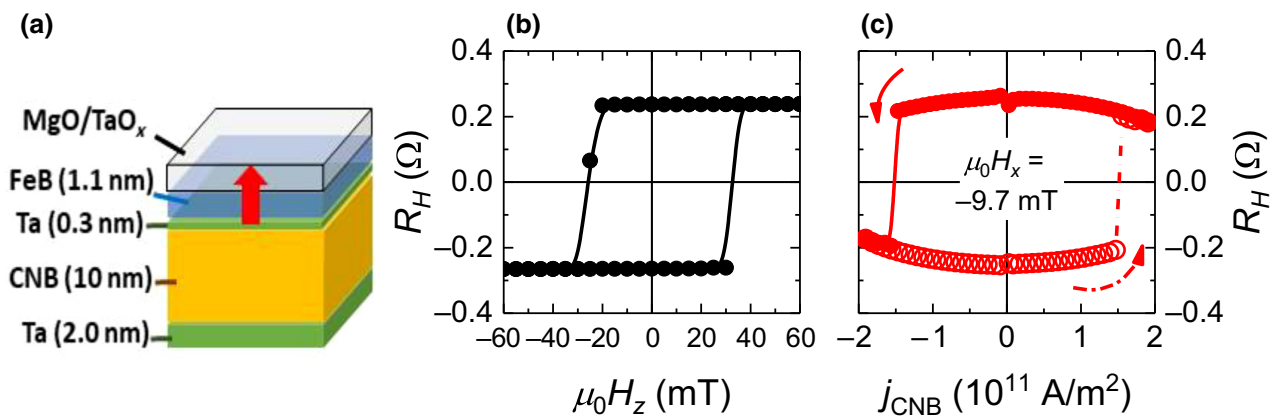


FIG. 6. SOT-induced magnetization switching. (a) Schematic of magnetic stack (arrow shows magnetization vector of Fe-B layer). (b) Hall resistance curve under Hz. (c) Current-induced magnetization switching behavior generated by spin Hall effect of CNB layer. In-plane magnetic field of -9.7 mT is applied along x axis, the magnetic field of which is parallel to the $-x$ direction.

[Fig. 6(a)]: substrate/Ta(2)/CNB(10)/Ta(0.3)/Fe-B(1.4)/MgO/TaOx(2). Instead of Cu-N, we use 0.3-nm-thick Ta as a spacer layer to achieve strong perpendicular magnetic anisotropy (PMA). The sample is annealed at 250 °C for 10 min. We note that the crystallinity of CNB remains amorphous after this annealing process, as determined by XRD measurement. The strong PMA of Fe-B in our system is confirmed by a square anomalous Hall curve with a relatively high coercive field of about 27 mT [Fig. 6(b)]. In Fig. 6(c), we show the current-induced switching behavior under small in-plane field application of -9.7 mT on the x axis [corresponding to applying 9.7 mT parallel to the $-x$ direction in Fig. 3(a)]. The counterclockwise switching behavior under the negative in-plane field shows consistent results with the DL SOT-induced magnetization switching with a positive spin Hall angle from the underlayer material [2,4]. Because the spin Hall angle of Ta is negative [3,19], the SHE on the CNB layer is the dominant spin source of our system, rather than the SHE on the spacer layer. We also confirm that the polarity of the switching behavior reverses when a positive in-plane field is applied. The switching current density is estimated to be about 1.5×10^{11} A/m², which is comparable to that of Pt [4] and Pd [28]. In addition, we observe the same switching polarity and switching current density using the CNB/Cr/Fe-B structure. This indicates that the interfacial effect, such as the spin-orbit filtering effect [23] and REE [2], at the interface between CNB and the spacer layer is negligible compared with the SHE in CNB.

III. CONCLUSION

We investigate the SHE in paramagnetic Co-Ni-B alloys via spin-orbit torque measurements. The SOT measurements reveal a large spin Hall angle, θ_{SHE} , of about 0.1, despite no heavy elements being used. We estimate the spin Hall conductivity to be about $1.0 \times 10^3 \Omega^{-1} \text{cm}^{-1}$, which is about the same order of magnitude as spin Hall materials that use heavy elements. From the composition dependence, we find that the large θ_{SHE} originates from the intrinsic contribution of the SHE in paramagnetic Ni, which is consistent with the previous calculation results. Finally, we demonstrate SOT-induced magnetization switching driven by the SHE in Co-Ni-B alloys and observe a switching current density comparable to that of Pt. These results show that paramagnetic Ni-based alloys can potentially realize highly efficient and heavy-element-free SOT-based devices.

ACKNOWLEDGMENTS

We thank T. Yamamoto for technical help. This work is partly supported by JSPS KAKENHI (Grant No. 19J01643), JST CREST (Grant No. JPMJCR18T3), Japan. Part of this work is conducted at the AIST Nano-Processing Facility, supported by the Nanotechnology

Platform Program of the Ministry of Education, Culture, Sports, Science and Technology (MEXT), Japan.

APPENDIX: FIELDLIKE TORQUE AND OERSTED TORQUE

The t_{CNB} dependences of the torque efficiencies of Oersted torque and FL SOT (ξ_{Oe} and ξ_{FL}) are shown in Fig. 7. The Oersted torque efficiency is calculated from the Oersted field by estimating the electrical charge density of metallic layers under the Fe-B-free layer. $\xi_{\text{FL(Oe)}}$ is defined as $\xi_{\text{FL(Oe)}} = -2eM_s t \mu_0 H_{\text{FL(Oe)}} / \hbar j_{\text{CNB}}$. The FL SOT values show the opposite sign to the Oersted torque and the same sign as that of DL SOT. Because the torque efficiencies of ξ_{Oe} and ξ_{FL} compete with each other, the total torque ($\xi_{\text{Oe}} + \xi_{\text{FL}}$ shown in black data) is an order smaller than that of the DL SOT efficiency.

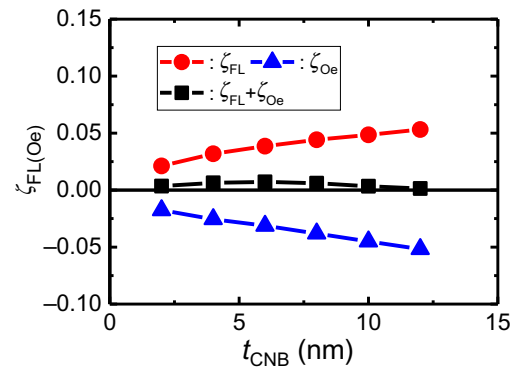


FIG. 7. t_{CNB} dependence of torque efficiencies of FL SOT (red), Oersted torque (blue), and total torque (black).

- [1] A. Manchon, J. Železný, I. M. Miron, T. Jungwirth, J. Sinova, A. Thiaville, K. Garello, and P. Gambardella, Current-induced spin-orbit torques in ferromagnetic and antiferromagnetic systems, *Rev. Mod. Phys.* **91**, 035004 (2019).
- [2] I. M. Miron, K. Garello, G. Gaudin, P.-J. Zermatten, M. V. Costache, S. Auffret, S. Bandiera, B. Rodmacq, A. Schuhl, and P. Gambardella, Perpendicular switching of a single ferromagnetic layer induced by in-plane current injection, *Nature* **476**, 189 (2011).
- [3] L. Liu, C.-F. Pai, Y. Li, H. W. Tseng, D. C. Ralph, and R. A. Buhrman, Spin-torque switching with the giant spin hall effect of tantalum, *Science* **336**, 555 (2012).
- [4] L. Liu, O. J. Lee, T. J. Gudmundsen, D. C. Ralph, and R. A. Buhrman, Current-Induced Switching of Perpendicularly Magnetized Magnetic Layers Using Spin Torque From the Spin Hall Effect, *Phys. Rev. Lett.* **109**, 096602 (2012).
- [5] J. Sinova, S. O. Valenzuela, J. Wunderlich, C. H. Back, and T. Jungwirth, Spin hall effects, *Rev. Mod. Phys.* **87**, 1213 (2015).

- [6] L. Liu, T. Moriyama, D. C. Ralph, and R. A. Buhrman, Spin-Torque Ferromagnetic Resonance Induced by the Spin Hall Effect, *Phys. Rev. Lett.* **106**, 036601 (2011).
- [7] W. Zhang, W. Han, X. Jiang, S. H. Yang, and S. S. P. Parkin, Role of transparency of platinum-ferromagnet interfaces in determining the intrinsic magnitude of the spin Hall effect, *Nat. Phys.* **11**, 496 (2015).
- [8] C. F. Pai, L. Liu, H. W. Tseng, D. C. Ralph, and R. A. Buhrman, Spin transfer torque devices utilizing the giant spin Hall effect of tungsten, *Appl. Phys. Lett.* **101**, 122404 (2012).
- [9] Y. Takeuchi, C. Zhang, A. Okada, H. Sato, S. Fukami, and H. Ohno, Spin-orbit torques in high-resistivity-W/CoFeB/MgO, *Appl. Phys. Lett.* **112**, 192408 (2018).
- [10] L. Zhu, D. C. Ralph, and R. A. Buhrman, Highly Efficient Spin-Current Generation by the Spin Hall Effect in Au_{1-x}Pt_x, *Phys. Rev. Appl.* **10**, 031001 (2018).
- [11] L. Zhu, K. Sobotkiewicz, X. Ma, X. Li, D. C. Ralph, and R. A. Buhrman, Strong damping-like spin-orbit torque and tunable dzyaloshinskii-moriya interaction generated by Low-resistivity Pd_{1-x}Pt_x alloys, *Adv. Func. Mater.* **29**, 1805822 (2019).
- [12] T. Naito, D. S. Hirashima, and H. Kontani, Tight-binding study of anomalous hall effect in ferromagnetic 3d transition metals, *Phys. Rev. B* **81**, 195111 (2010).
- [13] D. Jo, D. Go, and H. W. Lee, Gigantic intrinsic orbital hall effects in weakly spin-orbit coupled metals, *Phys. Rev. B* **98**, 214405 (2018).
- [14] C. Du, H. Wang, F. Yang, and C. Hammel, Systematic variation of spin-orbit coupling with *d*-orbital filling: Large inverse spin hall effect in 3d transition metals, *Phys. Rev. B* **90**, 140407(R) (2014).
- [15] T. Wang, W. Wang, Y. Xie, M. A. Warsi, J. Wu, Y. Chen, V. O. Lorenz, X. Fan, and J. Q. Xiao, Large spin hall angle in vanadium film, *Sci. Rep.* **7**, 1306 (2017).
- [16] M. W. Keller, K. S. Gerace, M. Arora, E. K. Delczeg-Czirjak, J. M. Shaw, and T. J. Silva, Near-unity spin hall ratio in Ni_xCu_{1-x} alloys, *Phys. Rev. B* **99**, 214411 (2019).
- [17] F. E. Luborsky, Composition dependence of the Curie temperatures of amorphous alloys, *J. Appl. Phys.* **51**, 2808 (1980).
- [18] M. Vázquez, A. Hernando, and O. V. Nielsen, Magnetostriction and other magnetic properties of Co-Ni based amorphous alloys, *J. Magn. Mag. Mater.* **61**, 390 (1986).
- [19] Y. Kato, Y. Saito, H. Yoda, T. Inokuchi, S. Shirotori, N. Shimomura, S. Oikawa, A. Tiwari, M. Ishikawa, M. Shimizu, B. Altansargai, H. Sugiyama, K. Koi, Y. Ohsawa, and A. Kurobe, Improvement of Write Efficiency in Voltage-Controlled Spintronics Memory by Development of a Ta-B Spin Hall Electrode, *Phys. Rev. Appl.* **10**, 044011 (2018).
- [20] Y. Fang, J. Persson, C. Zha, J. Willman, and C. W. Miller, Utility of reactively sputtered Cu_{Nx} films in spintronics devices, *J. Appl. Phys.* **111**, 073912 (2012).
- [21] C. O. Avci, K. Garello, M. Gabureac, A. Ghosh, A. Fuhrer, S. F. Alvarado, and P. Gambardella, Interplay of spin-orbit torque and thermoelectric effects in ferromagnet/normal-metal bilayers, *Phys. Rev. B* **90**, 224427 (2014).
- [22] M. Hayashi, J. Kim, M. Yamanouchi, and H. Ohno, Quantitative characterization of the spin-orbit torque using harmonic hall voltage measurements, *Phys. Rev. B* **89**, 144425 (2014).
- [23] S. C. Baek, V. P. Amin, Y. W. Oh, G. Go, S. J. Lee, G. H. Lee, K. J. Kim, M. D. Stiles, B. G. Park, and K. J. Lee, Spin currents and spin-orbit torques in ferromagnetic trilayers, *Nat. Mater.* **17**, 509 (2018).
- [24] E. Derunova, Y. Sun, C. Felser, S. S. P. Parkin, B. Yan, and M. N. Ali, Giant intrinsic spin Hall effect in W₃Ta and other A15 superconductors, *Sci. Adv.* **5**, eaav8575 (2019).
- [25] Y. Omori, E. Sagasta, Y. Niimi, M. Gradhand, L. E. Hueso, F. Casanova, and Y. C. Otani, Relation between spin Hall effect and anomalous Hall effect in 3d ferromagnetic metals, *Phys. Rev. B* **99**, 014403 (2019).
- [26] D. J. Wei, Y. Niimi, B. Gu, T. Ziman, S. Maekawa, and Y. Otani, The spin Hall effect as a probe of nonlinear spin fluctuations, *Nat. Commun.* **3**, 1058 (2012).
- [27] Y. Ou, D. C. Ralph, and R. A. Buhrman, Strong Enhancement of the Spin Hall Effect by Spin Fluctuations Near the Curie Point of Fe_xPt_{1-x} Alloys, *Phys. Rev. Lett.* **120**, 097203 (2018).
- [28] A. Ghosh, K. Garello, C. O. Avci, M. Gabureac, and P. Gambardella, Interface-Enhanced Spin-Orbit Torques and Current-Induced Magnetization Switching of Pd/Co/AIO_x Layers, *Phys. Rev. Appl.* **7**, 014004 (2017).